CrossMark

ELSEVIER

Experimental and Numerical Investigations on the Effect of Different Air-Fuel Mixing Strategies on the Performance of a Lean Liquid Fueled Swirled Combustor

Maria Grazia De Giorgi*, Aldebara Sciolti, Stefano Capilongo, Antonio Ficarella

University of Salento, Department of Engineering for Innovation, Via per Monteroni, Lecce 73100, Italy

Abstract

In the present work the performance of a multipoint lean direct injection strategy for low emission aero-propulsion systems has been experimentally and numerically investigated, and compared with the single point injection strategy. A swirler liquid fueled combustor was designed and used in experiments to investigate the flame behavior in lean and ultra-lean conditions for both the single-point and the multi-points injection strategies. Multipoint injection has been realized injecting an amount of fuel upstream the swirler inlet and using also the central injector as a "pilot" injection.

As regarding the experimental facilities, the combustor is equipped with four optical accesses for high speed flame imaging and with pressure and temperature sensors. Experimental data on flame characteristics and pollutant emissions are obtained. The characterization of the flame was realized using intensified high rate CCD camera for the acquisition in the ultraviolet spectral range. In front of the camera various combinations of optical filters were installed to selectively record the respective chemiluminescent species (OH* and CH*).

Computational fluid dynamic (CFD) simulations were also performed for a deeper understanding of the flame characteristics under the two injection strategies. The typical combustor operations were reproduced to more deeply understand the differences between the injection modes and the related flame patterns. The numerical results show different temperature and species fields predicted for the non-premixed and the partially premixed cases and furnish relevant information about the fluid dynamics in the combustion chamber in both the injection conditions.

1. Introduction

The development of low NOx gas turbine engine combustors is a main research issue. The amount of NOx depends on the flame temperature. Hence lean combustion strategy, which leads to reduction of combustion temperature, is of great interest [1].

The most remarkable problem of this combustion strategy is the insurgence of flame holding problems: instabilities, flashback or blowout (LBO) ([2], [3]) with negative effects on the combustor endurance and performance ([4]-[6]).

The flame stability under lean conditions is a serious problem in particular for lean liquid fueled combustor ([8]-[10]).

Lean premixed combustion including lean direct injection [11] and lean premixed pre-vaporized [12] is known as a possibility to reach lower NO_X emissions.

In this context since multipoint injection leads to a fast and efficient mixing, this is also a good candidate for lowering combustor

* Corresponding author. Tel.: +39-0832-297759; fax: +39-0832-297711.
E-mail address: mariagrazia.degiorgi@unisalento.it

emissions. However, its dynamic has to be deep investigated in order to underline its impact on flame stabilization, which is yet to be fully understood.

At this aim the signals experimentally acquired could be opportunely analyzed for extract useful information. Measurement techniques could include mass flow meters, thermocouples, pressure transducers, and probes for exhaust-gas composition measurements. However, more valuable and robust techniques, to provide direct information of the flame behavior, are based on chemiluminescence imaging measurements ([7], [13]-[16]). Furthermore real-time LBO control takes advantages from the acquisition of UV single specie emission images ([17]-[18]) or broadband emission [22]. Chemiluminescence signal from OH*, CH* and CO_2* species can be collected using an intensified camera equipped with different UV optical filtered and used for different analysis on the flame behavior ([19]-[23]).

Numerical investigations could be also used to support the experimental observations and to better understand the effects of operating conditions and injection strategies on the flame dynamics ([24]-[26]). Reddy et al. [27], used the CFD code Fluent-14.5 to develop a high intensity swirl based ultra-low emission flameless combustor with liquid fuels. Patel et al. [28] numerically investigated a liquid-fueled lean-direct injection (LDI) individuating the features that influence the spray dispersion. Jones et al. [29] numerically investigated the turbulent mixing, fuel spray dispersion and evaporation and combustion in a gas-turbine combustor.

Tyliszczak et al. [30] realized some numerical simulations of combustion process in a gas turbine with a single and multi-point fuel injection system.

In the present work, a liquid fuel burner was investigated under different operating conditions and two injection strategies, the single point injection and multipoint injections. The flame behavior at conditions close to LBO has been investigated using high speed imaging acquisitions. A high rate CCD camera, equipped with an intensifier and different optical filters, has been used for acquisitions in the ultraviolet spectral ranges of the chemiluminescence emissions from OH* and CH*. Moreover CFD simulations of the typical combustor operation conditions were also taken into account for a more deep analysis.

2. Detail of experimental methodology

2.1. The experimental set up and combustor geometry

The Green Engine Lab of University of Salento (Italy) is equipped with a 300 kW liquid-fueled swirling gas-turbine derived combustor ([31], [32]), shown in Fig. 1. The combustion chamber, which is reported in Fig. 2, has an internal diameter of 0.14 m and a length of 0.29 m. Preheated air enters from one site of the burner head and then splits in two ways: a coaxial one (primary air) and a swirled one (secondary air, eight-septa 45° swirler). Two different injection strategies could be applied. In the single injection (configurations 1A, 1B and 1C) the fuel is injected directly into the chamber using a central injector (one hole, 0.5 mm diameter), while in the multipoint injection (configurations 2A and 2B) the fuel is injected also through eight holes, one for each septa of the air swirler along a circumference of 0.075 m of diameter, 0.5 mm diameter. Figures 1b and 2b show the localization of the injection points in the multipoint configuration.
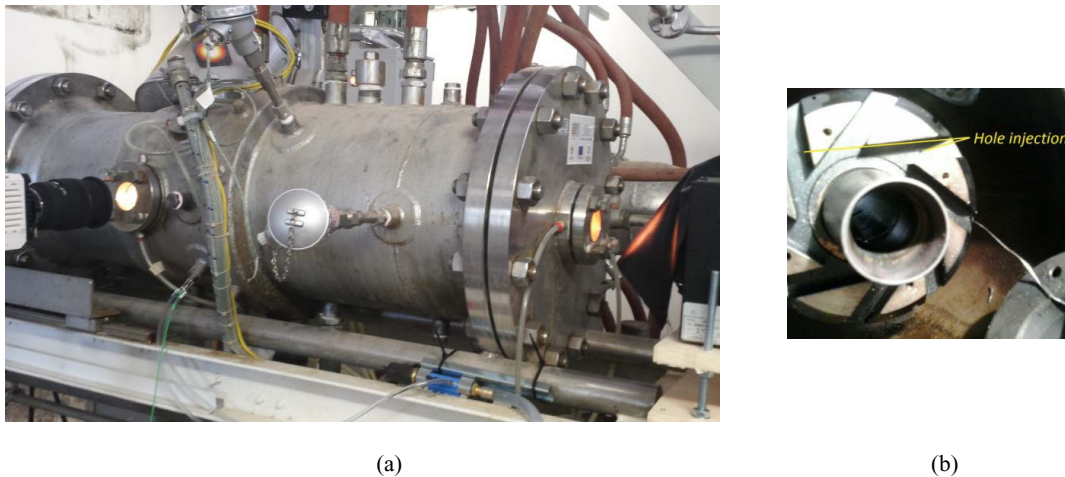

(a)   (b)

Fig. 1. (a) The Green Engine burner and (b) the particular of the injection holes.
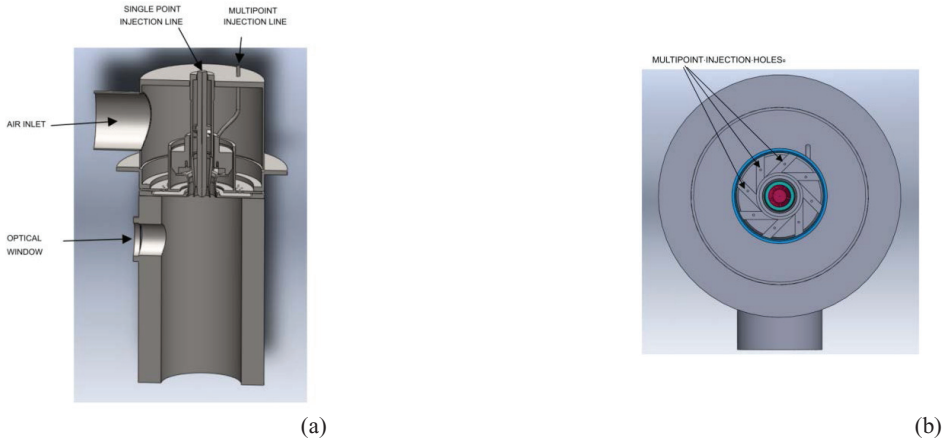
(a)   (b)

Fig. 2. (a) Green Engine burner scheme; (b) Details of the multipoint injection holes.

2.2. The experimental conditions

The air may be preheated up to 700 K and the pressure in the chamber (without combustion) may reach 3.5 bar$_a$, but in the present work the air at the inlets was set at 500 K and 1 bar$_a$. The fuel and air mass flow rates were set in order to investigate ultra lean conditions.

The total air flow rate was fixed at about $85 \cdot 10^{-3}$ kg/s with a ratio of 1:11 between primary and secondary air flow respectively. The fuel was injected from the central injector and/or the eight swirler injectors in different amounts, as summarized in Table . The ratio PR between the fuel mass flow rate in the premixing line (total flow rate of the 8 circumferential holes) and the total fuel mass flow rate has been used to quantify the level of the premixedness. Each variation of the fuel/air equivalent ratio was maintained for a 10 min interval, to ensure both stabilization of the equivalence ratio around the target value and steady state thermal boundary conditions.

The equivalence ratio Φ is defined as following:

$$\Phi = \frac{\left(m_{fuel} \middle/ m_{air} \right)}{\left(m_{fuel} \middle/ m_{air} \right)_{stoichiometric}} \tag{1}$$

Table 1: Test conditions.

CASE	Injection Configuration	AIR [g/s]	FUEL [g/s]		PR	Φ
			Central injector	8 injection points		
1A	Single point	83.92	1.81	0	0	0.348
1B	Single point	84.23	1.54	0	0	0.266
1C	Single point	86.10	1.30	0	0	0.219
2A	Multipoint	84.45	1.58	0.42	21%	0.344
2B	Multipoint	85.51	1.10	0.20	16%	0.219

2.3. Experimental measurements technique

The cooled optical accesses of the combustor, three circumferential and one frontal optical windows, permit to use imaging technique for the flame characterization acquiring the visible and the UV chemiluminescence emissions.

OH* and CH* chemiluminescence emissions images were acquired from the frontal windows of the burner by using the Phantom Miro M320S® High-Speed Digital Camera [33] equipped with an intensifier by Lambert Instrumentation® [34] and two interference filters with central wavelength of 307 nm and 431 nm respectively, with a full width at half maximum (FWHM)

of 10 nm. The intensifier gain was set to 250 for the CH* and 600 for the OH* emissions. The sensitivity and the quantum efficiency (QE) of the Intensifier are respectively 70 mA/W e 28% for the OH* acquisition and 74 mA/W and 21% for the CH*.

The UV images were taken with a resolution of 651 pixels x 407 pixels, a frequency of 1 kHz and a flame view area of 59 mm (h) and 36.8 mm (v).

Finally the pollutant emissions were also measured through a complete analyzer system (PG-350E Horiba) [35] equipped with gas sampling, sample conditioning, analyzer and system control units was used.

3. Detail of computational modeling

The computational analysis was carried out using the ANSYS Fluent 14.5 code. 3-D double-precision pressure-based solver was used with the Realizable k-ε model and the steady state assumption. The computations were performed assuming a fully developed combustion process, hence ignition and flame propagation processes were not taken into account. The spatial discretization was performed using the second-order upwind scheme. The SIMPLER algorithm was used for pressure–velocity coupling. The solution was assumed convergent when the scaled residual reached the level 10^{-5}.

The energy equation was solved considering 20 intermediate species equilibrium chemistry and a non-premixed droplet combustion model for simulating the combustion of the liquid fuels. Compressible flow was considered and the viscosity was calculated using Sutherland's law. A P1 radiation model was used. Constant mass-flow inlet condition normal to the boundary surface was applied at air inlets, and a pressure outlet based boundary condition was applied at the exit. No-slip wall and constant temperature boundary conditions were applied at the walls, based on experimental temperature values. The discrete phase trajectory for evaporating droplets is found by a Discrete Particle Model (DPM) using a Lagrangian formulation. Mass, momentum and energy exchanges for the droplets are calculated by integrating across control volumes while the interaction of the droplets with the continuous phase is also taken into account. A single component surrogate, $C_{10}H_{22}$ was used to simulate the fuel with a density of 730 kg/m^3. Fuel injection was simulated as a solid cone type spray with a cone half-angle of 20° and a radius of 0.00025 mm and a Rosin-Rammler drop size distribution with maximum, minimum and mean-droplet diameter's equal to 0.0005m, 0.0002m and 0.000001m respectively. Turbulent dispersion of particles is modelled with a discrete random walk model.

A number of computations were carried out using hexahedron mesh, shown in Fig.3, with approximately 2.15 million of cells, which was considered sufficient to obtain grid-independent results. The grid convergence was calculated based on the Grid Convergence Index (GCI) criteria. Three grids with different refinement levels (1149980, 2150167 and 3254033 cells) were compared. If the GCI for two successive grid sizes was below 3%, it was considered that grid convergence has been achieved.
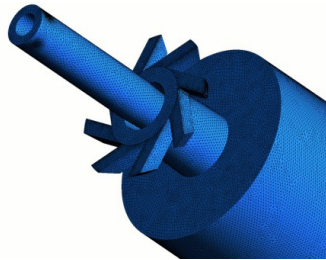

Fig. 3: Computational grid

4. Results

4.1. Results of the numerical investigations

Preliminary CFD simulations have been done to deeper investigate the differences between the two injection configurations at different fuel/air ratio.

Figure 4 reports the predicted contours of the temperature, mean mixture fraction, $C_{10}H_{22}$ mass fraction and OH* mass fraction in a vertical mid-plane for the two injection strategies at the same fuel/air ratio (case 1A and case 2A). Results underline that the flame is established closest to the main central fuel injector in case 2A. The location of the flame root is significant for the flame stability, hence this could lead to a better flame stability to blowout in the case of multipoint injection strategy.

A conical flame is predicted extending around the recirculation zone. This flame produces hot gases at a temperature close to 2200 K for the case 1A and approximately 2000 K for the case 2A. These gases do not mix immediately with the surrounding cold flow, resulting in a radially inhomogeneous temperature distribution in the first half of the chamber. Hence as expected, the temperature increased from the walls to the center line of the combustor.

In the second half part of the combustion chamber the computed mean temperature profile is relatively flat, the temperature

become more uniform in radial direction, due to the mixing with the cold flow, this leads to a significant decrease of the temperature at the chamber exit. with rising distance from the injection location. In the case A the overall temperature of the combustor as well as the maximum temperature is higher in the case 1A due to locally richer mixture.

Looking at the mean mixture fraction, it is evident where the vaporized fuel exists in the gas phase. It is significant in the fuel-rich portions of the flame. The small regions of fuel vapour close to central injector suggest that the vaporized fuel rapidly mixes with the oxidizer before undergoing chemical reactions.

Furthermore although the central region close is richer in the case 1A, moving axially downstream the mean mixture fraction is higher for the case 2A. The OH* emission contours are in good agreement with the temperature fields.
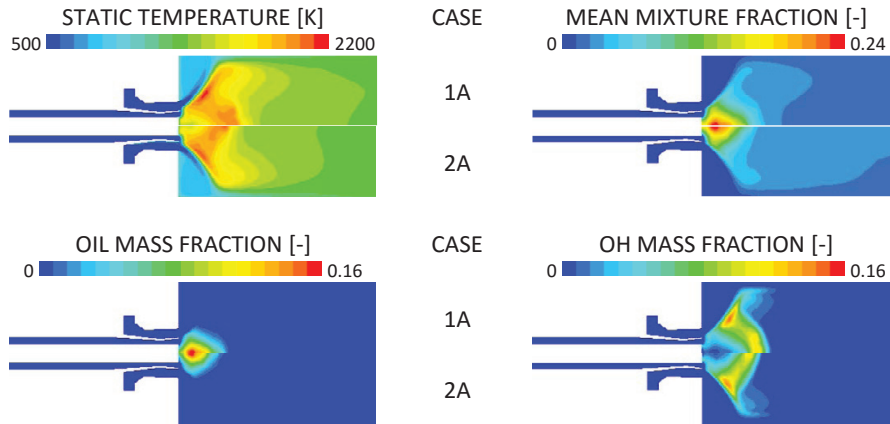

Fig. 4: Predicted contours of the temperature, mean mixture fraction, $C_{10}H_{22}$ mass fraction and OH* mass fraction in a vertical mid-plane for the two injection strategies at the same fuel/air ratio (case 1A and case 2A)
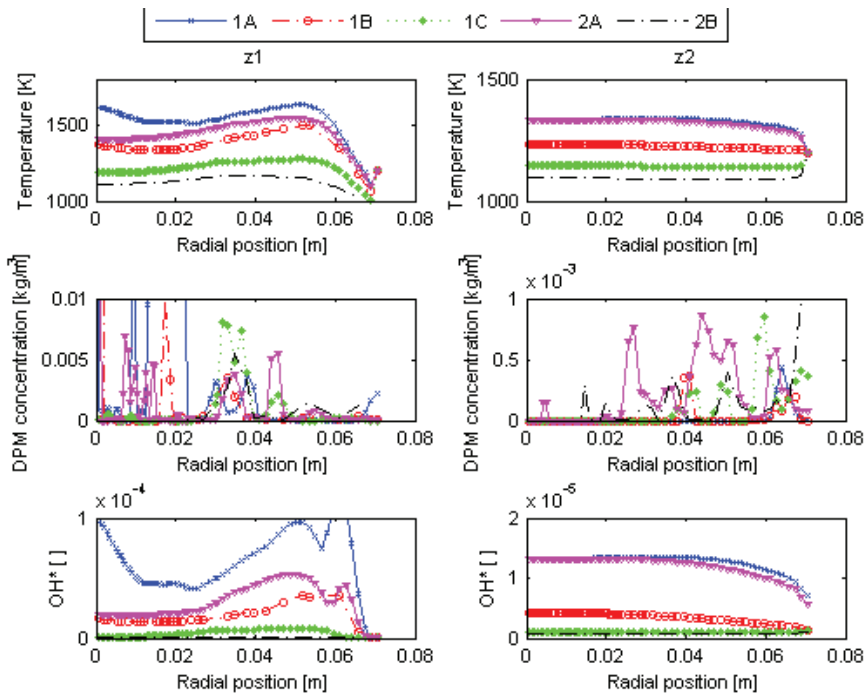

Fig. 5: Radial profiles of the predicted temperature, droplet concentration and OH* emissions at two axial distances 0.08 m and 0.22 m from the swirled exit, for the different test cases

Experimental results

The CO and NOx emissions were measured for the operating conditions that are reported in Table 1 and the measured values are shown in Fig.6.

In presence of a leaner combustion strategy the NOx emissions are sensibly reduced, this is in agreement with the overall reduction of the temperature, as shown also by the numerical simulations. The reduction of the fuel/air ratio permits a decrease of 25% and 34% in NOx emissions for respectively the non-premixed and partially premixed modes. Hence the main goal is better achieved by the partially-premixed combustion mode with multipoint injection.

As regarding the CO emissions, also in this case a decrease with the fuel reduction is recorded. For the multipoint injection the CO emission is always higher than in the single injection strategy. Hence the strong reduction (about 70%) that can be obtained with the fuel/air ratio reduction appears very interesting. With a higher availability of oxygen in the mixture the reaction can be completed more easily.
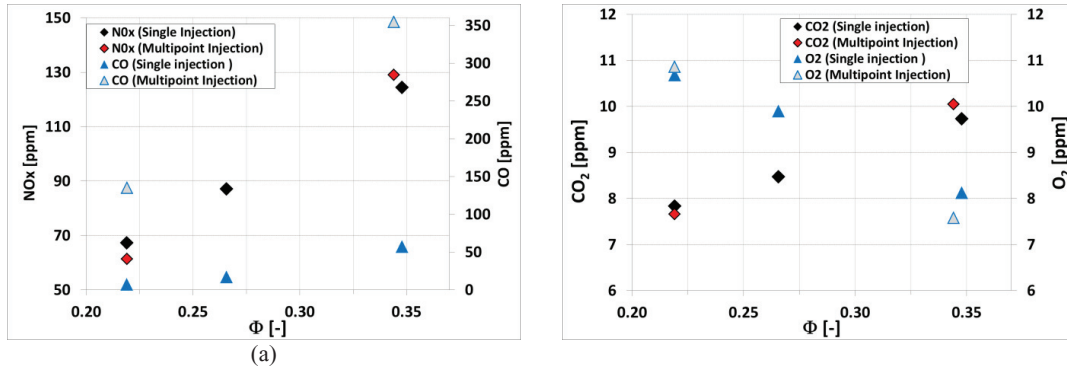

(a)
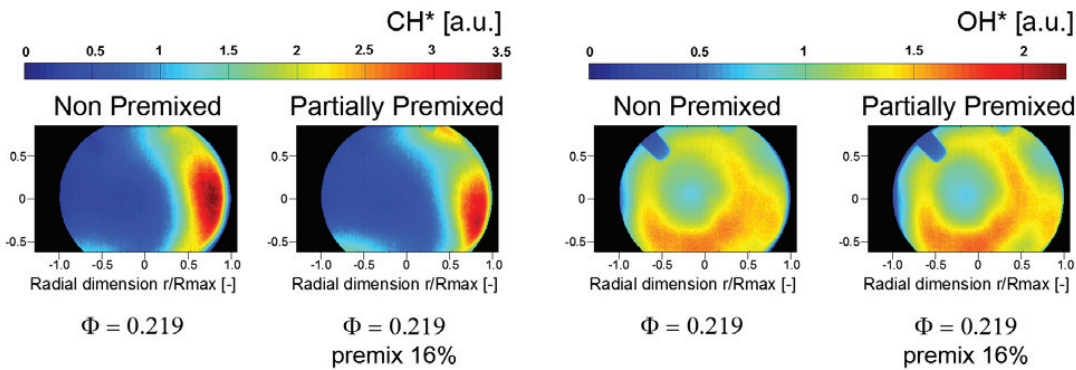
Fig. 6: Exhaust gas emissions

Fig. 7: Experimental time averaged values maps for (a) CH* and (b) OH* chemiluminescence emissions.

The maps obtained by the time averaged chemiluminescence emissions data are shown in Fig.7. As said before, the images are taken from the frontal windows. Hence, taking the longitudinal axis of the combustion chamber as reference (position [0,0] in the images), the coordinates are reported as distance from that axis in mm. It should be said that the protrusion, visible in the ICCD map, is a thermocouple.

The OH* and CH* intensities exhibit a strong concentration on the peripheral region while the central zone appears less interested by the reaction evolution. This trend may be remarked by the profiles in Fig.8 that makes evident this effect. This behaviour is also underlined by the numerical simulations, as shown in the OH* profiles in Fig.5. It is possible to observe that this effect may be connected with the swirl functioning.

Fixing the air mass flow rate, the radial profiles of OH* chemiluminescence intensity from the temporally averaged images are well correlated with the total fuel mass flow rate (or fuel/air ratio). Increasing the fuel mass flow rate the total heat release should also increase. Regarding the cases with the same injection strategy and different fuel/air ratios (case 1A vs case 1C, and

case 2A vs case 2C), Fig. 8 shows that, lowering the fuel/air ratio, there is a decrease of the OH* chemiluminescence intensity in the inner part of the flame and a slightly increase of the intensity close to the wall.

Regarding the time averaged CH* radial profiles, the CH* is radially more uniform for the cases at highest fuel/air ratio, while a relevant rise of the intensity in the peripheral zones is evident for the lean cases, in both the injection configurations.

Table 2 reports the spatially average values of the OH* and CH* emissions. It is evident the decrease of OH* and CH* lowering the fuel/air ratio as well as the reduction of these emissions if an amount of the total fuel is injected in the swirler vanes, with respect to the single point injection.
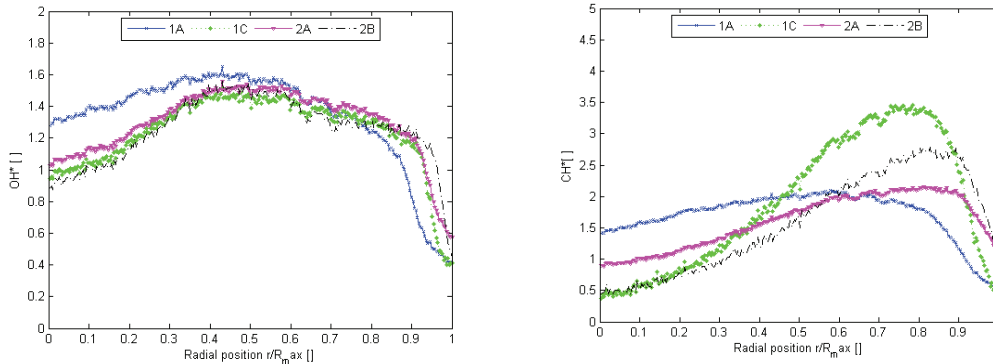

Fig. 8: (a) OH* and (b) CH* integrated chemiluminescence emissions profiles

Table 2: Spatially averaged OH* and CH* chemiluminescence emissions

CASE	OH*	CH*	Φ
1A	1.07	1.13	0.348
1B	1.01	1.02	0.266
1C	0.99	1.022	0.219
2A	1.02	1.06	0.344
2B	0.98	0.91	0.219

4. Conclusions

The paper presented an experimental and numerical study on a swirler liquid fueled in order to investigate the flame behavior in lean and ultra-lean conditions for both the single-point and the multi-points injection strategies.

Experimental data on flame characteristics and pollutant emissions are obtained. Experiments underline that for both the injection strategies, if the fuel/air ratio is lowered there is a decrease of the OH* chemiluminescence intensity in the inner part of the flame and a slightly increase of the intensity close to the wall. Furthermore the average values of the OH* and CH* emissions also decrease. Regarding the comparison between the two injection strategies the reduction of these emissions is higher if an amount of the total fuel is injected in the swirler vanes, with respect to the single point injection. Furthermore the reduction of the fuel/air ratio permits a decrease of 25% and 34% in NOx emissions for respectively the non-premixed and partially premixed modes.

Simulations were also performed for a deeper understanding of the flame characteristics under the two injection strategies. The numerical results show different temperature fields predicted for the single point and the multipoint injection cases and furnish relevant information about the fluid dynamics of the fluids ways in the combustion chamber in both the injection conditions.

The computations underline that the flame is established closest to the main central fuel injector in case of multipoint injection, this could lead to a better flame stability to blowout. Furthermore the maximum temperature is higher in the single injection due to locally richer mixture. The predicted OH* emission contours are in good agreement with the temperature fields and the experimental observations.

References

[1] W. Lazik, T. Doerr, S. Bake, R. v. d. Bank, and L. Rackwitz, "Development of Lean-Burn Low-NO," in Volume 3: Combustion, Fuels and Emissions, Parts A and B, 2008, pp. 797–807.
[2] M. Füri, P. Papas, and P. a. Monkewitz, "Non-premixed jet flame pulsations near extinction," Proc. Combust. Inst., vol. 28, no. 1, pp. 831–837, 2000.
[3] L. Rosentsvit, Y. Levy, V. Erenburg, V. Sherbaum, V. Ovcharenko, B. Chudnovsky, A. Herszage, and A. Talanker, "Extension of the Combustion Stability Range in Dry Low NO x Lean Premixed Gas Turbine Combustor Using a Fuel Rich Annular Pilot Burner," J. Eng. Gas Turbines Power, vol. 136, no. 5, p. 051509, Jan. 2014.
[4] K. U. Schildmacher, R. Koch, and H. J. Bauer, "Experimental characterization of premixed flame instabilities of a model gas turbine burner," Flow, Turbul. Combust., vol. 76, no. 2, pp. 177–197, 2006.
[5] M. Matalon, "Intrinsic Flame Instabilities in Premixed and Nonpremixed Combustion," Annu. Rev. Fluid Mech., vol. 39, no. 1, pp. 163–191, 2007.
[6] G. Campa and S. M. Camporeale, "Prediction of the Thermoacoustic Combustion Instabilities in Practical Annular Combustors," J. Eng. Gas Turbines Power, vol. 136, no. 9, p. 091504, 2014.
[7] J. Ballester, A. Sanz, and M. A. González, "Investigation of the characteristics and stability of air-staged flames," Exp. Therm. Fluid Sci., vol. 32, no. 3, pp. 776–790, 2008.
[8] M. G. De Giorgi, A. Sciolti, S. Campilongo, and A. Ficarella, "Assessment of the Combustion Behaviour of a Pilot-Scale Gas Turbine Burner Using Image Processing," in Proceedings of the ASME 2014 Power Conference, 2014, vol. 1, p. V001T01A001.
[9] M. G. De Giorgi, A. Sciolti, E. Pescini, and A. Ficarella, "Frequency Analysis and Predictive Identification of Flame Stability by Image Processing," in Proceedings of the 8th International Conference on Energy Sustainability Sustainable Cities and Communit, 2014, vol. 2, p. V002T04A014.
[10] M. Ruao, M. Costa, and M. Carvalho, "A NO x diagnostic system based on a spectral ultraviolet/visible imaging device," Fuel, vol. 78, no. x, pp. 1283–1292, 1999.
[11] Tacina, Robert, et al. "A Low NOx Lean-Direct Injection, Multipoint Integrated Module Combuster Concept for Advanced Aircraft Gas Turbines." (2002) Technical Report, Conference on Technologies and Combustion for a Clean Environment; 9-12 Jul. 2001; Oporto; Portugal.
[12] Bernier, D., F. Lacas, and S. Candel. "Instability mechanisms in a premixed prevaporized combustor." Journal of propulsion and power 20.4 (2004): 648-656.
[13] R. Hernández and J. Ballester, "Flame imaging as a diagnostic tool for industrial combustion," Combust. Flame, vol. 155, no. 3, pp. 509–528, 2008.
[14] B. U. Töreyin, Y. Dedeoğlu, U. Güdükbay, and a. E. Çetin, "Computer vision based method for real-time fire and flame detection," Pattern Recognit. Lett., vol. 27, no. 1, pp. 49–58, 2006.
[15] A. Tuntrakoon and S. Kuntanapreeda, "Image-based flame control of a premixed gas burner using fuzzy logics," Lect. Notes Artif. Intell. (Subseries Lect. Notes Comput. Sci., vol. 2871, no. 4, pp. 673–677, 2003.
[16] D. Sun, G. Lu, H. Zhou, and Y. Yan, "Condition Monitoring of Combustion Processes Through Flame Imaging and Kernel Principal Component Analysis," Combust. Sci. Technol., vol. 185, no. 9, pp. 1400–1413, 2013.
[17] J. Ballester and T. García-Armingol, "Diagnostic techniques for the monitoring and control of practical flames," Prog. Energy Combust. Sci., vol. 36, no. 4, pp. 375–411, 2010.
[18] J. Ballester, R. Hernández, A. Sanz, A. Smolarz, J. Barroso, and A. Pina, "Chemiluminescence monitoring in premixed flames of natural gas and its blends with hydrogen," Proc. Combust. Inst., vol. 32, no. 2, pp. 2983–2991, 2009.
[19] T. Yi and D. a. Santavicca, "Flame Spectra of a Turbulent Liquid-Fueled Swirl-Stabilized Lean-Direct Injection Combustor," 47th AIAAASMESAEASEE Jt. Propuls. Conf. Exhib., no. January, pp. 1–17, 2009.
[20] S. Keshav, Y. G. Utkin, M. Nishihara, J. W. Rich, I. V. Adamovich, and A. Bao, "Studies of Chemi-Ionization and Chemiluminescence in Supersonic Flows of Combustion Products," J. Thermophys. Heat Transf., vol. 22, no. 2, pp. 157–167, 2008.
[21] C. Allouis, R. Pagliara, and A. Saponaro, "Fast infrared imaging for combustion stability analysis of industrial burners," Exp. Therm. Fluid Sci., vol. 43, pp. 2–8, 2012.
[22] G. P. Smith, J. Luque, C. Park, J. B. Jeffries, and D. R. Crosley, "Low pressure flame determinations of rate constants for OH(A) and CH(A) chemiluminescence," Combust. Flame, vol. 131, no. 1–2, pp. 59–69, Oct. 2002.
[23] C. Allouis, F. Beretta, A. Ferrante, and A. Saponaro, "Fast Infrared Imaging To Study Industrial Burner Combustion," Proc. Eur. Combust. Meet., 2009.
[24] A. Akbari, S. Hill, V. McDonell, and S. Samuelsen, "Experimental and Computational Analyses of Methane and Hydrogen Mixing in a Model Premixer," J. Eng. Gas Turbines Power, vol. 133, no. 10, p. 101503, Oct. 2011.
[25] A. Akbari, S. Hill, V. McDonell, and S. Samuelsen, "Statistical Evaluation of CFD Predictions of Measured Mixing Properties of Hydrogen and Methane for Lean Premixed Combustion," Vol. 2 Combust. Fuels Emiss. Parts A B, no. x, pp. 939–949, 2011.
[26] S. Ruan, N. Swaminathan, T. Isono, T. Saitoh, and K. Saitoh, "Simulation of Premixed Combustion with Varying Equivalence Ratio in Gas Turbine Combustor," J. Propuls. Power, vol. 31, no. 3, pp. 861–871, 2015.
[27] V. M. Reddy, A. Katoch, W. L. Roberts, and S. Kumar, "Experimental and numerical analysis for high intensity swirl based ultra-low emission flameless combustor operating with liquid fuels," Proc. Combust. Inst., vol. 35, no. 3, pp. 3581–3589, 2015.
[28] N. Patel, M. Kirtaş, V. Sankaran, and S. Menon, "Simulation of spray combustion in a lean-direct injection combustor," Proc. Combust. Inst., vol. 31 II, no. 2, pp. 2327–2334, 2007.
[29] W. P. Jones, A. J. Marquis, and K. Vogiatzaki, "Large-eddy simulation of spray combustion in a gas turbine combustor," Combust. Flame, vol. 161, no. 1, pp. 222–239, Jan. 2014.
[30] A. Tyliszczak, A. Boguslawski, D. Nowak, "Numerical simulations of combustion process in a gas turbine with a single and multi-point fuel injection system", Applied Energy 174 (2016) 153–165
[31] M. G. De Giorgi, A. Sciolti, S. Campilongo, and A. Ficarella, "Image processing for the characterization of flame stability in a non-premixed liquid fuel burner near lean blowout," Aerospace Science and Technology, vol. 49, pp. 41–51, 2016.
[32] M. G. De Giorgi, A. Sciolti, S. Campilongo, and A. Ficarella, "Experimental data regarding the characterization of the flame behaviour near lean blowout in a non-premixed liquid fuel burner," Data Br., vol. 6, pp. 189–193, 2016.
[33] "Phantom M320 CCD specifications." [Online]. Available: https://www.abelcine.com/store/Phantom-Miro-M320S-High-Speed-Digital-Camera/.
[34] VV. AA., "High-Speed Intensified Camera Attachment specifications." Online available: http://www.lambertinstruments.com/hicatt.
[35] VV. AA., "Horiba PG 350 specifications." Online available: http://www.horiba.com/uk/process-environmental/products/combustion/details/pg-350e-portable-gas-analyzer-19617/.
[36] VV. AA., "Fluent 14.5 user's guide." Online available: http://www.ansys.com/Support/Documentation.